International Journal of Engineering Trends and Technology
ISSN: 2231–5381 / https://doi.org/10.14445/22315381/IJETT-V73I7P111

Volume 73 Issue 7, 127-137, July 2025

Original Article

Power Loss Analysis of SHE-PWM Controlled Modified Modular Multilevel Converter

Preeti Kapoor[1*], Sonali Rangari[1], Gaurav Goyal[1], Pragati Shrivastava Deb[2], Mohan Renge[3]

[1]*Department of Electrical Engineering, Shri Ramdeobaba College of Engineering and Management, Maharashtra, India.*
[2]*Department of Electrical and Computer Engineering, ABES Engineering College, Uttar Pradesh, India.*
[3]*Department of Electrical Engineering, Visvesvaraya National Institute of Technology (VNIT), Maharashtra, India.*

[1*]*Corresponding Author : kapoorpv@rknec.edu*

Received: 24 March 2025 Revised: 18 June 2025 Accepted: 25 June 2025 Published: 30 July 2025

Abstract *- The Modular Multilevel Converter (MMC) has emerged as a leading topology in the power converter family, attracting extensive global research and development interest. This paper presents a modified configuration of the MMC. In the modified configuration, an attempt has been made to replace the submodule capacitance with a separate DC source. The number of DC sources required is also reduced as lower submodules share a common DC link. The '2N+1' level modulation technique has been employed to further reduce the number of submodules required to achieve the desired output voltage level. Due to its superior performance characteristics, the Modular Multilevel Converter (MMC) is a popular choice for high-power, medium-voltage applications. The converter efficiency in high-power applications is the paramount aspect. Therefore, the analysis of power loss must be conducted at the initial stage of converter design. For the induction motor control drive, the power loss calculation method in the bridge modified configuration of MMC is also presented in the paper. The method includes the calculation of conduction loss and switching loss. Energy dissipation through conduction of the MMC submodule depends upon duty cycle, load current, and power factor, whereas power losses caused by switching depend upon switching frequency. The converter has been controlled by applying the Selective Harmonic Elimination Pulse Width Modulation (SHE-PWM) technique. In addition, the study presents a comparative evaluation of SHE-PWM and SPWM modulation techniques based on simulation results obtained under different operating scenarios. The proposed structure of three-phase three-level MMC has been analyzed, implemented and verified by developing a laboratory prototype controlling a low-power induction motor drive rated 746W, 415V. The experimental results of the modified configuration of MMC and power loss estimation that were presented confirm the simulated results.*

Keywords - *Modular multilevel converter, SHE-PWM, Induction motor, Conduction loss, Switching loss.*

1. Introduction

Modular Multilevel Converters (MMCs) are increasingly favoured for medium- and high-voltage power conversion applications, owing to their scalable architecture, superior output voltage quality, and modular design [1, 2]. Features of MMC is high power quality of current and voltage, having high voltage rating, high modularity and higher efficiency, have create the MMC a standard option and solution for numerous applications together with Static Compensators (STATCOMs), large scale PV plants, high-voltage dc transmission, motor drives High Voltage Direct Current (HVDC) transmission, Grid-connected renewable energy systems, and electric drives and Medium Voltage (MV) grid [3-10]**.** The Modular Multilevel Converter (MMC) is widely used in high-power, medium-voltage applications to realize the Double Star Chopper Cell (DSCC) topology, facilitating advanced research and development efforts. The DSCC-based topology was first introduced in 2003 as in [11]. MMC provides several advantages, including modularity, scalability to meet high-voltage and high-power demands, superior power quality, fault-tolerant operation, enhanced reliability, and higher overall efficiency [12, 13]. Modulation strategies in MMC are also the subject of intense research. The original implementation of the Modular Multilevel Converter (MMC) utilized the Space Vector Modulation (SVM) technique, as presented in [11]. However, as the levels increase, this technique becomes increasingly complex. Therefore, multi-carrier-based modulation techniques [14, 15] are commonly preferred due to their simplicity and effectiveness. The commonly used multicarrier modulation technique requires 'N' carriers for 'N' connected submodules in each arm to generate a phase-to-neutral output voltage with 'N+1' levels. Some multicarrier modulation strategies are based on interleaving, using 2N carriers to generate a high-level output voltage, i.e. '2N+1' [16]. In high-power systems, Selective Harmonic Elimination PWM (SHE-PWM) is advantageous as

it enables effective harmonic suppression with considerably reduced switching frequency, enhancing efficiency and reducing switching losses. This method uses the Fourier series expansion method to form a nonlinear transcendental equation. Different methods are suggested in the literature to solve these equations, as explained in [17-20]. By solving transcendental equations to target and eliminate specific low-order harmonics, SHE-PWM achieves effective reduction in Total Harmonic Distortion (THD), all while operating at comparatively lower switching frequencies, making it well-suited for high-power applications. This characteristic makes it especially advantageous for MMCs, where each submodule's switching activity significantly contributes to overall power loss. In this work, the Selective Harmonic Elimination PWM (SHE-PWM) method is utilized to govern the switching operation, and its effectiveness is assessed through detailed performance analysis.

Designing a Modular Multilevel Converter (MMC) entails determining the suitable ratings of power semiconductor devices, selecting an appropriate switching frequency, and sizing passive components accordingly. Accurate power loss estimation plays a vital role in the design process of power converters, directly influencing efficiency, thermal management, and overall system performance. During the operation of a power switch, four primary types of losses can occur: (i) switching loss, (ii) off-state loss, (iii) gate drive loss, and (iv) switching loss. Among these, off-state and gate losses are typically minimal and are therefore neglected in the analysis.

As the Modular Multilevel Converter (MMC) is predominantly employed in medium-voltage, high-power applications, the power semiconductor devices used are rated for high voltage and current levels, making conduction and switching losses the primary contributors to overall power loss. An online modeling approach for accurate assessment of conduction and switching losses in cascaded H-bridge multilevel inverters was proposed by Alamri et al. [21]. The analytical approach to calculating multilevel converter losses is too complicated and requires more commutation [22, 23]. This online model is simple and easy to implement for loss calculation. This paper focuses on calculating switching loss and conduction loss using the online method.

The study further investigates the switching frequencies necessary to eliminate identical harmonic orders when employing SPWM and SHE-PWM modulation strategies. This work presents a comparative evaluation of power losses and converter efficiency for SPWM and SHE-PWM methods, considering the Elimination of harmonics of identical Order. Simulation is also carried out on R-L load for different power factors with different modulation index. A three-phase, three-level Modular Multilevel Converter (MMC) was experimentally implemented and tested under laboratory conditions to validate its functionality. The prototype was developed to run a phase 1 HP, 415V, 2A, 1440 rpm rated induction motor. As the digital controllers offer flexibility and adaptability, the control circuit was designed with the help of the digital control processor. In addition to the control circuit, the gate drive circuit uses ultra-high-speed driver MIC4425 for driving an IGBT with a maximum current rating of 25 A and blocking voltage of 1200 V, which is used in the three-phase three-level MMC. Experimental observations were obtained using a TPS2024B digital oscilloscope. Experimental results are presented by applying the modulation strategy SHE-PWM to a three-phase three-level MMC. The result presented verifies the successful operation of a phase three-level MMC driving a phase induction motor.

The paper's main contribution is as follows: Section 1 introduces the Modular Multilevel Converter (MMC), outlining its key advantages, practical applications, and appropriate modulation strategies. Section 2 discusses the fundamental structure and operation of the MMC. Section 3 presents the functioning of the modified three-phase, three-level MMC configuration. Section 4 explains the selective harmonic elimination technique and its comparison with the Sinusoidal Pulse Width Modulation (SPWM) technique. Section 5 describes the power loss estimation method; Section 6 presents the comparison of SHE-PWM with the SPWM technique. Section 7 presents hardware implementation, and its results are discussed. Section 8 presents the conclusion of the work done.

2. Basic Structure of MMC

The schematic of the three-phase Modular Multilevel Converter (MMC) is provided in Figure 1 to illustrate its fundamental structure. Each phase leg comprises lower and upper arms composed of submodules that can be configured as full-bridge or half-bridge circuits.

As the number of switches required in a full bridge configuration is almost double that of a half-bridge configuration, it results in higher switching losses and confers certain advantages. The half-bridge configuration is more often developed as the number of required semiconductor devices is smaller. Hence, an MMC with a half-bridge configuration is used throughout the paper for analysis.

Each arm of the MMC consists of 'N' identical submodules linked in series, along with an arm inductance (Larm). The submodule serves as the fundamental building block of the MMC, providing its modular structure. As Figure 2 illustrates, each submodule in the half-bridge configuration comprises two identical switching devices and a submodule capacitor ‘C’. Switches S1 and S2 in each submodule operate complementarily: S1 ON implies S2 OFF and vice versa. When S2 is ON, the output voltage VO is zero; when S1 is ON, VO=VC, the capacitor voltage. If both switches are ON simultaneously, a short circuit across the capacitor is created,

posing a risk of damage. This mode of operation is prohibited. When both switches are OFF, the terminal voltage depends on the current direction through the submodule. Based on this current direction, the capacitor either charges or discharges.

The charging or discharging of the submodule capacitor is governed by the half-bridge switching state and the direction of the current flowing through the submodule. Table 1 provides a summary of the switching states, possible arm current directions, terminal voltages of the half-bridge submodule, and the corresponding capacitor charging or discharging conditions. During the positive half cycle (iarm>0), upper arm capacitors always charge, while the lower capacitors discharge. During the negative half-cycle (iarm < 0), the capacitors in the upper arm discharge, whereas those in the lower arm are charged.

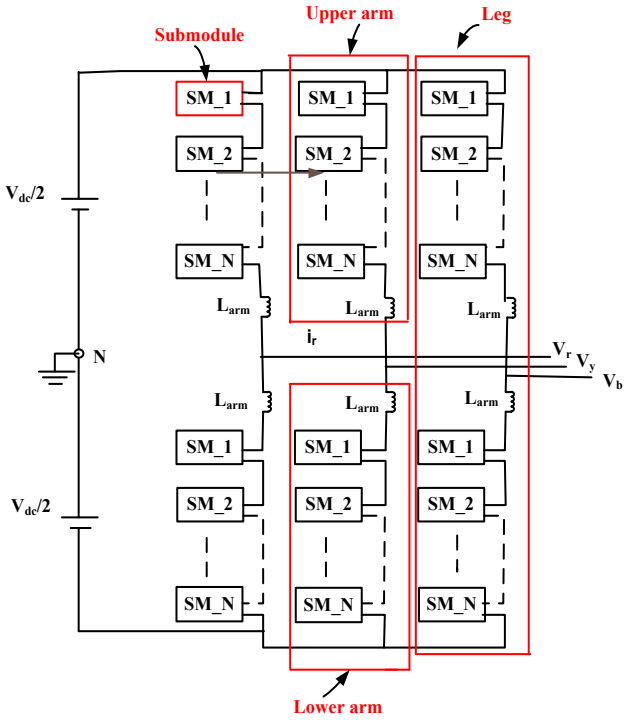

Fig. 1 Basic configuration of three-phase MMC

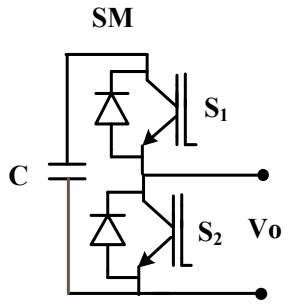

Fig. 2 Schematic of half-bridge submodule

Table 1. Working of the submodule

Switching States / Current Direction	S_1 = ON, S_2 = OFF	S_2 = ON, S_1 = OFF	Capacitor State
$i_{arm} > 0$	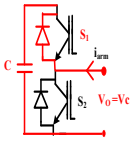	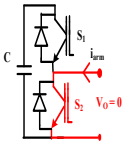	(a) Charging (b) State remains unchanged
$i_{arm} < 0$	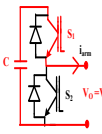	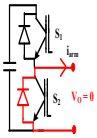	(c) Discharging (d) State remains unchanged

3. Modified Configuration of MMC

Capacitor voltage balancing in submodules is a critical control challenge in MMCs, as the submodule capacitor voltages and internal circulating currents are closely coupled within the same phase leg, complicating the control strategy. The various modulation and controlling strategies have been suggested in [24-27] to balance the capacitor voltage and suppress circulating current. Separate DC sources are used to develop a submodule to overcome the problem of submodule capacitor balancing.

The lower submodules are driven by a common DC source, leading to a reduction in the number of discrete DC sources necessary for operation. This configuration is feasible due to the shared DC bus among the lower submodules, as depicted in Figure 1. Hence, considering the above problems, a new configuration of MMC topology to generate a three-level output with *N*=1 submodule in each leg is proposed as represented in Figure 3. Although a similar topology using a voltage source was proposed in 1981 [20], the capacitor-based MMC was first commercialized by R. Marquardt, as noted in [11].

Modified MMC configuration does not have a DC source midpoint, hence the phase-to-neutral voltage cannot be realized. Therefore, the number of levels in MMC cannot be investigated with the nature of the phase to neutral voltage. However, from the levels generated by the line voltage waveform, it can be said that the proposed configuration of MMC generates a three-level phase-to-neutral voltage output. Figure. Figure 3 depicts a three-level MMC configuration enabling seven distinct switching states to generate a five-level line-to-line voltage waveform. Table 2 presents the voltage levels along with their corresponding switch states, clearly indicating the working of the proposed MMC configuration, generating positive voltage levels (i.e +Vdc and +Vdc/2), negative voltage levels (i.e. -Vdc and -Vdc/2) and zero level. A logic value of '1' denotes the switch's active or ON state, whereas '0' indicates it is in the OFF state.

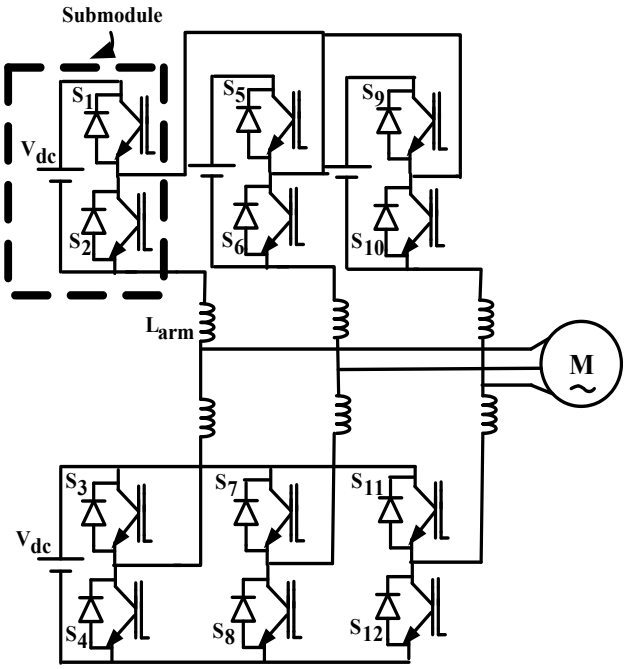

Fig. 3 Modified configuration of three-level MMC topology

Table 2. Switching combination of a proposed three-phase three-level MMC configuration

Line Voltage 'Vry'	Switching States							
	S1	S2	S3	S4	S5	S6	S7	S8
+Vdc	0	1	1	0	1	0	0	1
+Vdc/2	0	1	0	1	1	0	0	1
	0	1	1	0	0	1	0	1
0	0	1	0	1	0	1	0	1
-Vdc	1	0	0	1	0	1	1	0
-Vdc/2	0	1	0	1	0	1	1	0
	1	0	0	1	0	1	0	1

4. Selective Harmonic Elimination Pulse Width Modulation (SHE-PWM)

SHE-PWM operates without carrier signals and functions offline, enabling control of the fundamental voltage while removing particular harmonic components through direct computation of switching times. This approach enables the generation of high-quality output voltage at significantly lower switching frequencies, making it suitable for high-power applications.

The technique utilizes the Fourier series to express the harmonic components present in the PWM waveform analytically. A system of nonlinear equations is formulated to suppress the 5th, 7th, 11th, and 13th harmonics by analyzing the harmonic components of the output waveform. The optimal switching angles are obtained by solving these nonlinear equations using the Newton-Raphson (N-R) iterative technique. The N-R method program was developed using MATLAB software. The switching angles were computed for a modulation index varying from 0.1 to 1. For validation and testing, the angles $\alpha_1 = 9.390°$, $\alpha_2 = 20.530°$, $\alpha_3 = 35.070°$, $\alpha_4 = 65.780°$, and $\alpha_5 = 75.610°$ corresponding to a modulation index of 0.9 were selected.

The three-phase MMC configuration was simulated using MATLAB-SIMULINK to obtain a three-level output voltage waveform. The simulation parameters used are the same as those given in Table 3. A switching frequency of 500 Hz is selected to eliminate harmonic components up to the 13th Order effectively. For MI = 0.9, the corresponding switching angles are selected. Three-phase gating pulses are generated in MATLAB-SIMULINK based on the calculated switching angles and are subsequently applied to the three-phase MMC, resulting in a three-level output voltage. The waveforms of line voltage, line currents and speed of induction motor of three-level MMC employing SHE-PWM technique are shown in Figure 4. Simulation results show that speed drops when full load torque TL = 5 N-m is applied at 0.5 sec, with a simultaneous increase in the line currents.

Table 3. Simulation parameters of converter and motor

Motor Rating	1 HP, 415 V, 2 A, 1440 rpm
Stator resistance (R_s), leakage inductance (L_{ls})	14.8Ω, 0.0561 H
Rotor resistance (R_r), leakage inductance (L_{lr})	6.14mΩ, 0.0561 H
Mutual inductance (L_m)	0.538 H
Submodule voltage (V_{dc})	750 V
Arm inductance (L_{arm})	8 mH
Modulation Index (MI)	0.9

For the modified configuration of MMC, the SHE-PWM modulation approach is the most appropriate switching frequency to remove the Order of harmonic components. It is also observed that a 1050 Hz switching frequency is needed to remove harmonics up to the 13th Order, while a switching frequency of 500 Hz is needed in SHE-PWM to remove harmonics up to the same Order. It is also observed that the SHE-PWM modulation technique helps reduce the circulating current compared to the SPWM technique.

A variation in the number of inserted submodules within a converter leg leads to an imbalance between the phase legs, resulting in the flow of internal circulating currents. The circulating currents include a DC part and a prominent second harmonic component, both leading to greater losses in the converter's phase legs and requiring passive components with higher power ratings. A converter design considers a number of variables, including passive component design, switching frequency selection, and rating of the power semiconductor switch. Power loss is one of the most important practical considerations that might affect the design. Power electronics circuitry to control a drive requires switching semiconductor devices.

The power loss analysis in MMC is done through simulation and verified with hardware results using the SHE-PWM control approach. The results were compared and reported, indicating that MMC can benefit from a modulation approach that can lower overall power loss and increase converter efficiency.

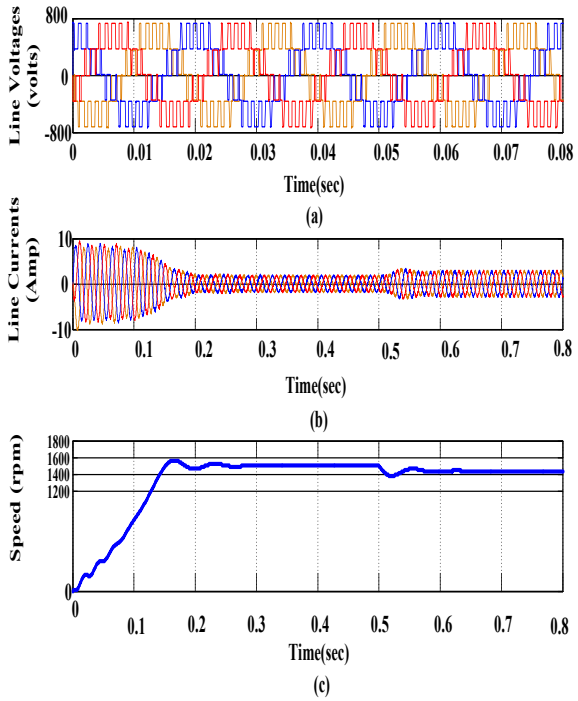

Fig. 4 Simulated results showing (a) Line voltage, (b) Line currents, and (c) Speed of IM of three-level MMC (SHE-PWM technique)

5. Power Loss Analysis

Any converter designed for high power applications must choose a semiconductor switch rating to optimize the switching frequency and the necessary size to reduce power loss. The work examines the mathematical calculation of switching and conduction losses using the SHE-PWM controlled three-level MMC driving a three-phase medium-voltage induction motor rated at 1.6 MW and 3.3 kV. It was found that a switch can handle up to 1000A of current, and the highest voltage rating for an IGBT in the market for this range of current is FZ1500R33HL3. Consequently, FZ1500R33HL3 type IGBT, which has a blocking voltage of a maximum current of 1500 A and 3.3 kV, is the switching device taken into consideration for the analysis [28]. IGBT voltage is typically de-rated to between 50% and 60%. Therefore, the voltage of the submodule is limited to 1.5 kV–2 kV by the 3.3 kV rating of the IGBT. Therefore, the results presented take into account the assumption that each submodule is made up of three switches connected in series.

5.1. Conduction Loss Estimation

When the switch is ON and conducting current, a loss occurs in the semiconductor switch. This occurs due to the voltage drop across the semiconductor switch while current flows through it. During conduction, the losses in the IGBT and freewheeling diode are calculated by multiplying their respective on-state or saturation voltages (VCE for the IGBT and VD for the diode) with the corresponding conduction current and anode current or the current passing through the collector (ID for the diode current and IC for the main switch current). Equation (1) is used to estimate the conduction power loss for IGBT, and by using Equation (2), the conduction loss of the diode is estimated.

$$P_{con-IGBT} = \frac{1}{T}\int_0^T [V_{ce} * I_c]dt \quad (1)$$

$$P_{con-Diode} = \frac{1}{T}\int_0^T [V_D * I_D]dt \quad (2)$$

Where the switching cycle is '*T*'.

The computation of the total conduction power losses is carried out as given in Equation (3):

$$P_{con-total} = P_{con-IGBT} + P_{con-Diode} \quad (3)$$

Under these operating conditions, the on-state voltage is represented by a quadratic expression derived from the on-state current, capturing the nonlinear behavior of the semiconductor device. The curve fitting tool in MATLAB-SIMULINK is employed to extract this quadratic relationship using actual device parameters from the datasheet, as summarized in Table 4.

This IGBT's datasheet can be found in [28]. Two quadratic equations, one for the diode and one for the IGBT, are connected to each device. The conduction loss calculation block diagram is displayed in Figure. 5.

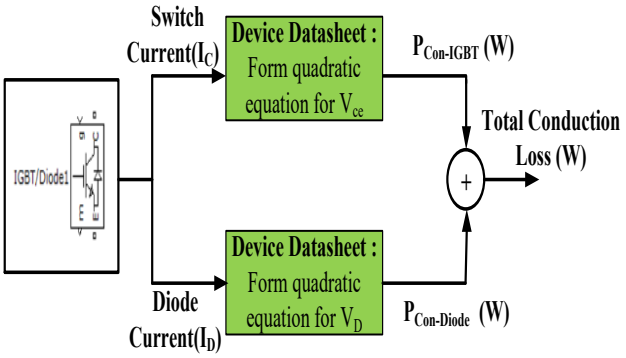

Fig. 5 Block diagram for conduction loss estimation

5.2. Switching Loss Estimation

Current commutation cannot happen instantly in real power semiconductors, switches experience high voltage and high current at the same time. Switching loss results from this situation. The loss arises when the electronic device is switched, especially when it is turned on and off. It occurs in

both diodes and IGBTs. Switching loss is caused by this situation. Switching loss information is shown in datasheets for diode reverse recovery (turn-off) graphs as $E_{rec\text{-}ID}$, for IGBT turn-on as $Ae_{on\text{-}IC}$, and $E_{off\text{-}IC}$ for IGBT turn-off. Due to the fast transition into conduction under forward-bias conditions, the associated turn-on losses of the diode are minimal and typically neglected in power loss calculations. Equations (4) and (5) quantify the main switch's turn-on and turn-off power losses, respectively, whereas Equation (6) estimates the reverse recovery power loss associated with the diode.

$$P_{on} = \frac{1}{T}\sum[E_{on} * I_c]f_s \quad (4)$$

$$P_{off} = \frac{1}{T}\sum[E_{off} * I_c]f_s \quad (5)$$

$$P_{rec} = \frac{1}{T}\sum[E_{rec} * I_D]f_s \quad (6)$$

Where f_s represents the switching frequency.

The overall switching power loss is determined using the following calculation.

$$P_{SW-Total} = P_{on} + P_{off} + P_{rec} \quad (7)$$

Overall, switching loss arises from the energy dissipated during the transitions of a switch from ON to OFF and OFF to ON states. This includes both turn-on and turn-off losses. Based on the device datasheet, an energy factor "K" can be derived, which represents the energy loss per unit current. It is calculated by dividing the switching energy loss by the corresponding switch current during the transition.

The Curve Fitting Tool in MATLAB-SIMULINK is employed to derive the quadratic equations for $K_{IGBT\text{-}OFF}$ and $K_{IGBT\text{-}ON}$ in terms of the state current. Similarly, using the real parameters listed in the device datasheet, the quadratic equation for $K_{Diode\text{-}rec}$ is computed in terms of diode current. Energy loss can be obtained by multiplying energy factor curves by switching current, and power loss is obtained by multiplying energy factor curves by switching frequency.

The normalization factor is utilised to compensate if the blocking voltage varies. Figure 6 illustrates the block diagram for calculating switching losses. Table 4 summarizes the mathematical equations derived for the selected IGBT switch through curve fitting analysis in MATLAB, accurately representing its operational characteristics. Ultimately, the total power loss is obtained by summing the individual switching and conduction losses, which are computed based on the fitted equations and corresponding operating conditions.

$$P_{loss-Total} = P_{con-Total} + P_{SW-Total} \quad (8)$$

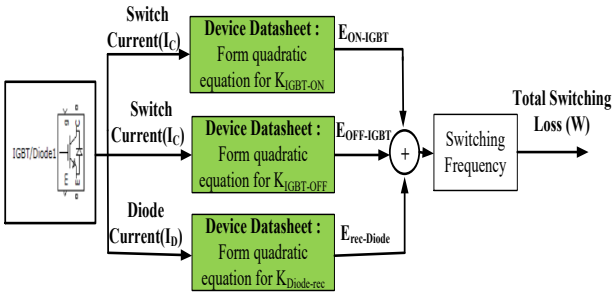

Fig. 6 Block diagram for switching loss estimation

Table 4. IGBT curve-fitting equation extracted from datasheet at 125℃ ambient temperature

$V_{ce} = -1.8 * 10^{-7} I_c^2 + 0.0016 * I_c + 0.99$
$V_D = -1.8 * 10^{-7} I_D^2 + 0.0013 * I_D + 0.73$
$K_{IGBT-ON} = 7.7 * 10^{-7} I_c^2 - 0.0023 * I_c + 3.9$
$K_{IGBT-OFF} = 4.9 * 10^{-7} I_c^2 - 0.002 * I_c + 3.8$
$K_{IGBT-rec} = 1.5 * 10^{-6} I_D^2 - 0.0069 * I_D + 8.6$

6. Comparative Analysis with SPWM Technique

The topology was independently simulated using SPWM and SHE-PWM techniques, each configured with appropriate switching frequencies to eliminate harmonic components up to the 13th Order. To eliminate 13th-order harmonics, the SPWM technique necessitates a switching frequency of 1050 Hz, whereas the SHE-PWM technique achieves the same harmonic Elimination at a lower switching frequency of 500 Hz. Figures 7 and 8 illustrate the simulated current waveforms of an individual submodule under SPWM and SHE-PWM control schemes, respectively. The MATLAB simulation model extracts the individual current waveforms corresponding to the IGBT and the freewheeling diode separately for detailed analysis. The on-state current of the device is analyzed to distinguish the conduction paths, where the positive portion indicates current through the IGBT and the negative portion corresponds to current through the diode. Based on the separately extracted current waveforms, the conduction losses of both the IGBT and the diode are evaluated using the method depicted in the block diagram shown in Figure 5. Likewise, the switching losses are computed following the methodology illustrated in Figure 6.

Table 5 presents a comparative analysis of the simulation results, focusing on the Elimination of harmonic components up to the 13th Order using both modulation techniques. The results demonstrate the relative effectiveness of each method in minimizing harmonic distortion, offering insights into their performance and suitability for different applications. Figures 7 and 8 clearly illustrate that the SHE-PWM technique is effective in reducing both switching and conduction losses, making it a more efficient option compared to the alternative method. The analysis reveals that SPWM requires nearly double the switching frequency compared to SHE-PWM to effectively suppress harmonic components up to the 13th Order, indicating higher switching stress and potential

efficiency drawbacks. Since higher switching frequency leads to increased switching losses, the overall converter losses using the SPWM technique are approximately three times greater than those observed with the SHE-PWM technique. Consequently, the use of the SHE-PWM technique results in a 3% improvement in converter efficiency.

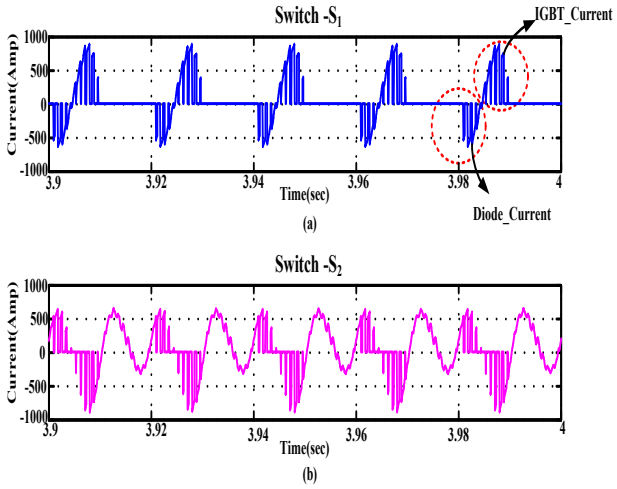

Fig. 7 SPWM-based current waveforms in one submodule, (a) Through the upper switch, and (b) Through the lower switch

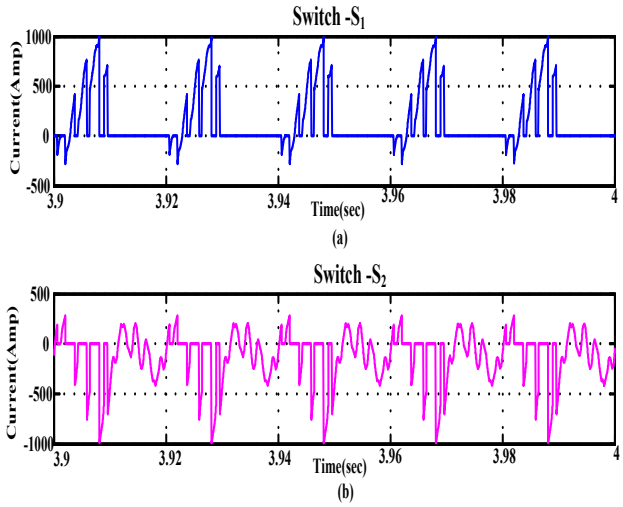

Fig. 8 Current waveforms through a single submodule using the SHE-PWM technique, (a) Upper switch current, and (b) Lower switch current

Table 5. Harmonic elimination (up to 13th order) - A comparative study of modulation methods

Comparison Parameter	SPWM Technique	SHE-PWM Technique
Switching frequency f_s	1050 Hz	500 Hz
Overall power loss [kW]	66.76	22.83
Inverter Power Loss Relative to Output Power [%]	4.17	2.15
Efficiency of Inverter [%]	95.99	98.58

6.1. Effect of Modulation Index and Power Factor on Inverter Efficiency

Simulation is further extended to study the effect of varying power factor with different modulation index on inverter efficiency. Figure 9 shows the 3-D graphical representation of percentage inverter efficiency versus power factor and modulation index with the SPWM technique. Figure 10 shows a comparative analysis of inverter efficiency with varying power factor and modulation index with the SPWM and SHE-PWM techniques. From Figure 9, it is clear that inverter efficiency remains the same for the considered modulation index for a particular power factor, but it decreases with a decrease in power factor for a particular modulation index. Figure 10 shows that the range of inverter efficiency is clearly greater with the SHE-PWM technique than with the SPWM technique.

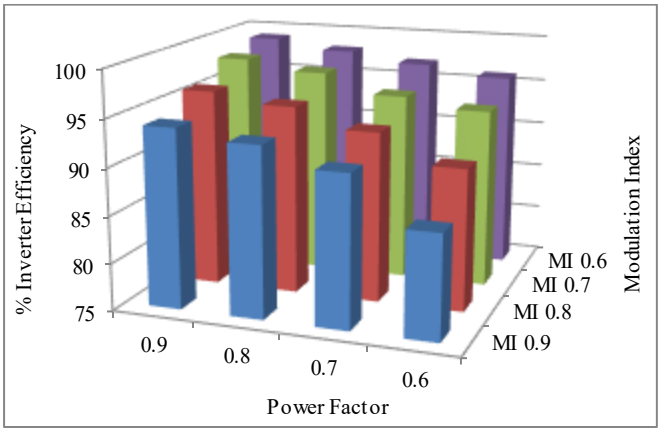

Fig. 9 Graphical representation of inverter efficiency vs power factor and modulation index with SPWM technique

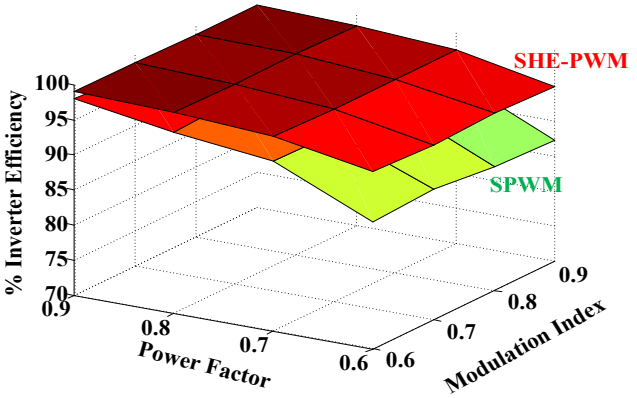

Fig. 10 Comparative analysis of inverter efficiency with power factor and modulation index with both the SPWM and SHE-PWM techniques

7. Validation of Modified Configuration of MMC

The three-phase three-level modular multilevel converter is fabricated in the laboratory to verify the operation. Prototype is developed to run a phase 1 HP, 415V, 2A, 1440

rpm rated induction motor as shown in Figure 11. As the digital controllers offer flexibility and adaptability, the control circuit was designed with the help of a digital control processor. The dsPIC33EP256MU810 microcontroller is used to get SHE-PWM pulses. MIC4425, the gate drive circuit with ultra-high speed for driving an IGBT having a maximum current rating of 25 A and a blocking voltage of 1200 V, is used in the three-phase three-level MMC. The TPS 2024B digital oscilloscope is used to capture experimental results. The result presented compares the simulated and hardware results and justifies the successful operation of a phase induction motor driving with three-phase three-level MMC.

Figure 12 illustrates the gate pulses derived from the computed switching angles for a single phase leg of the MMC, while Figure 13 demonstrates the 120° phase shift accomplished across all three phase legs. As shown in Figure 14, all line voltages of the induction motor exhibit a 120° phase shift.

The observed waveforms confirm that the number of voltage levels in the line voltage follows the relation '2n-1', where 'n' represents the number of levels in the phase voltage. An inverter is designed to generate a level output; the line voltage will always have five levels, and it is satisfied in the given results.

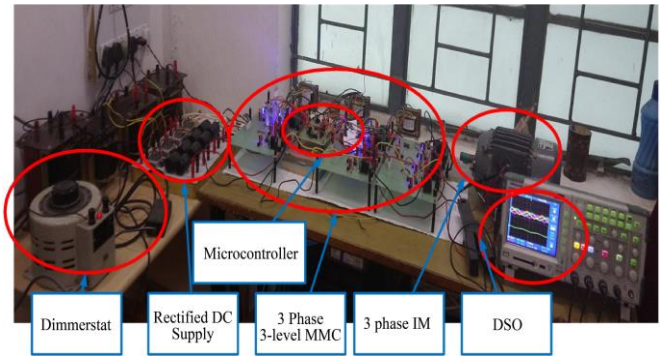

Fig. 11 Laboratory set-up of three-level MMC driving induction motor

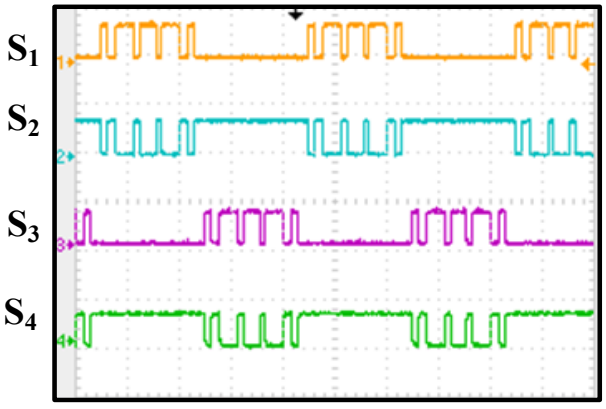

Fig. 12 Switching pulses for one phase-leg of MMC generated at pins of dsPIC33EP256MU810 microcontroller (Scale X-axis = 5 ms/div, Y-axis = 2 V/div)

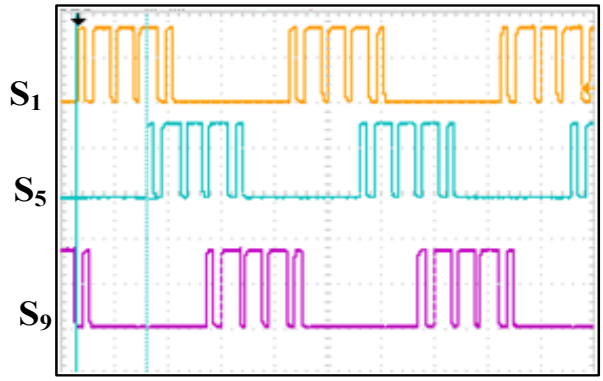

Fig. 13 Three-phase upper switch pulses in each arm (Scale X-axis = 5.0 ms/div and Y-axis = 2 V/div)

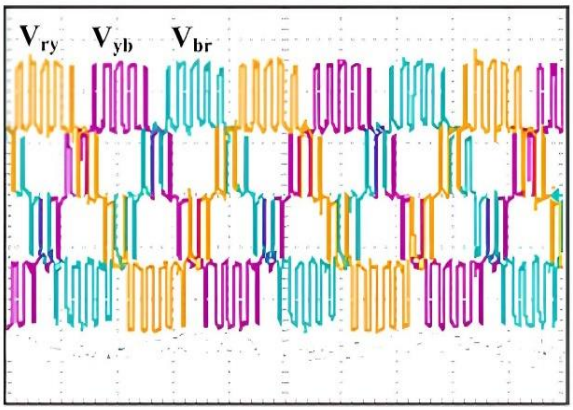

Fig. 14 Line voltages of IM (Scale X-axis = 5 ms/div, Y-axis = 50 V/div for voltage)

The phase line currents of the induction motor, as shown in Figure 15, show a 120^0 phase shift.

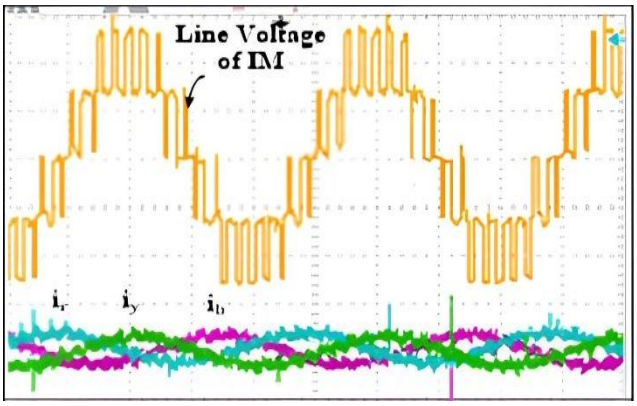

Fig. 15 Line voltage and three phase currents of IM (Scale X-axis = 5 ms/div, Y-axis = 50 V/div for voltage and Y-axis = 100 A/div for current)

7.1. Experimental Verification of Power Loss

Power loss of one sub-module for the modified MMC configuration is calculated in experimentation, and the results were compared with simulated values. Referring to the datasheet, IGBT, quadratic equations are obtained in MATLAB-SIMULATION employing the curve fitting tool

from real characteristics specified in the datasheet. Based on the curve fitting equations shown in Table 4, conduction and switching losses were estimated per the method given in the block diagram shown in the Figures 4 and 5, respectively. Figure 16 illustrates the simulated voltage and current waveforms for switches S_1 (V_{S1} & I_{S1}) and S_2 (V_{S2} & I_{S2}) within a single submodule. The DC link voltage for each submodule in the simulation is set to 320 V. In the experimentation, voltage and current waveforms for S_1 (V_{S1} & I_{S1}) and S_2 (V_{S2} & I_{S2}) of one sub-module are captured in a digital storage oscilloscope as shown in Figure 17.

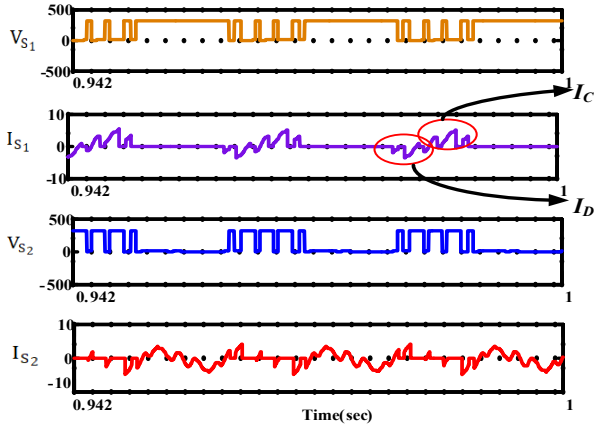

Fig. 16 Simulated results: voltage and current waveforms of one submodule

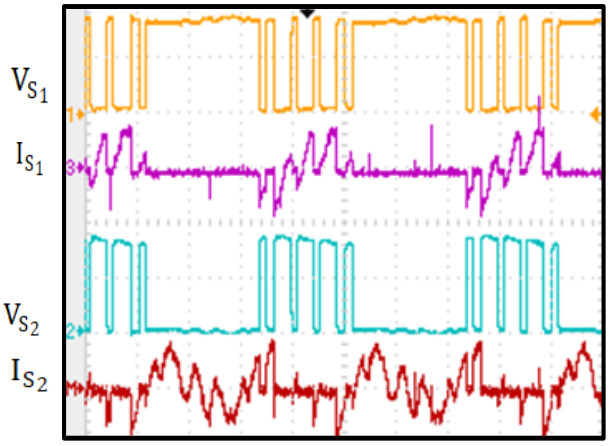

Fig. 17 Experimental results of single submodule voltage waveform and current waveform (Scale X-axis = 5 ms/div, Y-axis = 50 V/div)

The generated Excel sheet is used for further analysis. The product of (V_{S1} & I_{S1}) and (V_{S2} & I_{S2})gives the total power loss of S_1 and S_2, respectively. The sub-module input DC voltage is set to a value of 90V. The nature of waveforms obtained by simulation and experimental results is approximately matched. Comparative power loss analysis with simulation and experimental results is shown in Table 6. The simulated and experimental power loss results in one sub-module are observed to be approximately matched by applying a scaling factor.

Table 6. Comparison of simulated and experimental power loss values

Simulated Power Loss Values (W)						Experimental Value of Power Loss (W) at V_{dc} = 90V		
At V_{dc} = 320V			At V_{dc} = 90V (with scaling factor)					
S_1 Switch	S_2 Switch	Total	S_1 Switch	S_2 Switch	Total	S_1 Switch	S_2 Switch	Total
0.8950	1.5332	2.4282	0.2517	0.4312	**0.6829**	0.2993	0.3733	**0.6726**

8. Conclusion

The proposed configuration of a three-phase three-level MMC with DSCC configuration has been analyzed and successfully implemented in MATLAB-SIMULINK software operating a three-phase induction motor drive. The proposed configuration helps avoid the extra circuitry required for capacitor voltage balancing by replacing sub-module capacitance with a separate DC source. Furthermore, the lower arm submodules are powered by a shared DC source, effectively minimizing the total number of individual DC sources required. A laboratory prototype of a three-level Modular Multilevel Converter (MMC) driving a three-phase, 746 W, 415 V induction motor has been successfully developed and experimentally verified. The performance results closely match those obtained from the simulation. Implementation is carried out effectively by applying both the SHE-PWM modulation technique. Conduction and switching losses are the most prevalent types of losses. This study offers a straightforward, effective, and user-friendly software-based approach for assessing each device's conduction and switching losses. Converter efficiency is computed by adding the losses of each device to determine the overall loss. With the successful implementation and operation of the proposed configuration of three-phase three-level MMC operating at 415V and 746 W rated IM with SHE-PWM technique. Simulated and experimental power loss values of one sub-module are approximately matched by applying a scaling factor.

References

[1] Luis A.M. Barros, António P. Martins, and José Gabriel Pinto, "A Comprehensive Review on Modular Multilevel Converters, Submodule Topologies, and Modulation Techniques," *Energies*, vol. 15, no. 3, pp. 1-51, 2022. [CrossRef] [Google Scholar] [Publisher Link]

[2] JosÉ Rodriguez et al., "Multilevel Voltage-Source-Converter Topologies for Industrial Medium-Voltage Drives," *IEEE Transactions on Industrial Electronics*, vol. 54, no. 6, pp. 2930-2945, 2007. [CrossRef] [Google Scholar] [Publisher Link]

[3] Yumeng Tian et al., "Review, Classification and Loss Comparison of Modular Multilevel Converter Submodules for HVDC Applications," *Energies*, vol. 15, no. 6, pp. 1-32, 2022. [CrossRef] [Google Scholar] [Publisher Link]

[4] Marcelo A. Perez et al., "Modular Multilevel Converters: Recent Achievements and Challenges," *IEEE Open Journal of the Industrial Electronics Society*, vol. 2, pp. 224-239, 2021. [CrossRef] [Google Scholar] [Publisher Link]

[5] Amir Parastar, Yong Cheol Kang, and Jul-Ki Seok, "Multilevel Modular DC/DC Power Converter for High-Voltage DC-Connected Offshore Wind Energy applications," *IEEE Transactions on Industrial Electronics*, vol. 62, no. 5, pp. 2879-2890, 2014. [CrossRef] [Google Scholar] [Publisher Link]

[6] Maryam Saeedifard, and Reza Iravani, "Dynamic Performance of a Modular Multilevel Back-To-Back HVDC System," *IEEE Transactions on Power Delivery*, vol. 25, no. 4, pp. 2903-2912, 2010. [CrossRef] [Google Scholar] [Publisher Link]

[7] Ahmed Elsanabary, Saad Mekhilef, and Nur Fadilah Ab Aziz, "Internal Power Balancing of an MMC-Based Large-Scale PV System under Unbalanced Voltage Sags," *IEEE Journal of Emerging and Selected Topics in Power Electronics*, vol. 12, no. 4, pp. 3729- 3739, 2024. [CrossRef] [Google Scholar] [Publisher Link]

[8] Yang Wang et al., "A Review of Modular Multilevel Converters for Stationary Applications," *Applied Sciences*, vol. 10, no. 21, pp. 1-36, 2020. [CrossRef] [Google Scholar] [Publisher Link]

[9] Siba Kumar Patro, and Anshuman Shukla, "Modular Directed Series Multilevel Converter for HVDC Applications," *IEEE Transactions on Industry Applications*, vol. 56, no. 2, pp. 1618-1630, 2020. [CrossRef] [Google Scholar] [Publisher Link]

[10] Saud Alotaibi, and Ahmed Darwish, "Modular Multilevel Converters for Large-Scale Grid-Connected Photovoltaic Systems: A Review," *Energies*, vol. 14, no. 19, pp. 1-30, 2021. [CrossRef] [Google Scholar] [Publisher Link]

[11] Anton Lesnicar, and Rainer Marquardt, "An Innovative Modular Multilevel Converter Topology Suitable for a Wide Power Range," *2003 IEEE Bologna Power Tech Conference Proceedings*, Bologna, Italy, vol. 3, pp. 272-277, 2003. [CrossRef] [Google Scholar] [Publisher Link]

[12] Suman Debnath et al., "Operation, Control, and Applications of the Modular Multilevel Converter: A Review," *IEEE Transactions on Power Electronics*, vol. 30, no. 1, pp. 37-53, 2015. [CrossRef] [Google Scholar] [Publisher Link]

[13] Marcelo A. Perez et al., "Circuit Topologies, Modeling, Control Schemes, and Applications of Modular Multilevel Converters," *IEEE Transactions on Power Electronics*, vol. 30, no. 1, pp. 4-17, 2015. [CrossRef] [Google Scholar] [Publisher Link]

[14] B.P. McGrath, and D.G. Holmes, "Multicarrier PWM Strategies for Multilevel Inverters," *IEEE Transaction on Industrial Electonics*, vol. 49, no. 4, pp. 858-867, 2002. [CrossRef] [Google Scholar] [Publisher Link]

[15] Kalle Ilves et al., "Analysis and Operation of Modular Multilevel Converters with Phase-Shifted Carrier PWM," *IEEE Transactions on Power Electronics*, vol. 30, no. 1, pp. 268-283, 2015. [CrossRef] [Google Scholar] [Publisher Link]

[16] Georgios S. Konstantinou, Mihai Ciobotaru, and Vassilios G. Agelidis, "Analysis of Multi-Carrier PWM Methods for Back-To-Back HVDC Systems based on Modular Multilevel Converters," *IECON 2011 - 37th Annual Conference Proceedings on IEEE Industrial Electronics Society*, Melbourne, VIC, Australia, pp. 4391-4396, 2011. [CrossRef] [Google Scholar] [Publisher Link]

[17] Angel Pérez-Basante et al., "(2N+1) Selective Harmonic Elimination-PWM for Modular Multilevel Converters: A Generalized Formulation and A Circulating Current Control Method," *IEEE Transactions on Power Electronics*, vol. 33, no. 1, pp. 802-818, 2018. [CrossRef] [Google Scholar] [Publisher Link]

[18] Georgios Konstantinou, Mihai Ciobotaru, and Vassilios Agelidis, "Selective Harmonic Elimination Pulse-Width Modulation of Modular Multilevel Converters," *IET Transaction Power Electronics*, vol. 6, no. 1, pp. 96-107, 2013. [CrossRef] [Google Scholar] [Publisher Link]

[19] Hasmukh S. Patel, and Richard G. Hoft, "Generalized Techniques of Harmonic Elimination and Voltage Control in Thyristor Inverters: Part II---Voltage Control Techniques," *IEEE Transactions on Industry Applications*, vol. IA-10, no. 5, pp. 666-673, 2007. [CrossRef] [Google Scholar] [Publisher Link]

[20] Y. Sahali, and Mohammed-Karim Fellah, "Selective Harmonic Eliminated Pulse-Width Modulation Technique (SHE PWM) Applied to Three-Level Inverter/Converter," *Industrial Electronics, IEEE International Symposium on Industrial Electronics (Cat. No.03TH8692)*, Rio de Janeiro, Brazil, vol. 2, pp. 1112-1117, 2003. [CrossRef] [Google Scholar] [Publisher Link]

[21] Baseem Alamri, and Mohammad Darwish, "Power Loss Investigation for 13-Level Cascaded H-Bridge Multilevel Inverter," *Journal of Energy Power Sources*, vol. 2, no. 6, pp. 230-238, 2015. [Google Scholar]

[22] Baris Ciftci, and Ahmet M. Hava, "Performance Evaluation and Selection of PWM Switching and Control Methods for Grid Connected Modular Multilevel Converters," *2015 IEEE Energy Conversion Congress and Exposition (ECCE)*, Montreal, QC, Canada, pp. 3622-3629, 2015. [CrossRef] [Google Scholar] [Publisher Link]

[23] Tomas Modeer, Hans-Peter Nee, and Staffan Norrga, "Loss Comparison of Different Sub-Module Implementations for Modular Multilevel Converters in HVDC Applications," *(EPE) European Power Electronics and Drives Journal*, vol. 22, no. 3, pp. 32-38, 2012. [CrossRef] [Google Scholar] [Publisher Link]

[24] Maryam Saeedifard, and Reza Iravani, "Dynamic Performance of a Modular Multilevel Back To-Back HVDC System," *IEEE Transaction on Power Delivery*, vol. 25, no. 4, pp. 2903-2912, 2010. [CrossRef] [Google Scholar] [Publisher Link]

[25] Jiangchao Qin, and Maryam Saeedifard, "Reduced Switching-Frequency Voltage-Balancing Strategies for Modular Multilevel HVDC Converters," *IEEE Transactions on Power Delivery*, vol. 28, no. 4, pp. 2403-2410, 2013. [CrossRef] [Google Scholar] [Publisher Link]

[26] Kalle Ilves et al., "Predictive Sorting Algorithm for Modular Multilevel Converters Minimizing the Spread in the Submodule Capacitor Voltages," *IEEE Transactions on Power Electronics*, vol. 30, no. 1, pp. 440-449, 2015. [CrossRef] [Google Scholar] [Publisher Link]

[27] Zixin Li et al., "An Inner Current Suppressing Method for Modular Multilevel Converters," *IEEE Transaction on Power Electronics*, vol. 28, no. 11, pp. 4873-4879, 2013. [CrossRef] [Google Scholar] [Publisher Link]

[28] Infineon Technologies, FZ1500R33HL3, 3300 V, 1500 A Single Switch IGBT Module, 2025. [Online]. Available: https://www.infineon.com/cms/en/product/power/igbt/igbt-modules/fz1500r33hl3/